Available online at www.sciencedirect.com
SCIENCE DIRECT®
Journal of Catalysis 236 (2005) 9–13
JOURNAL OF CATALYSIS
www.elsevier.com/locate/jcat

Study of the interfacial structure of a Pt/α-Al_2O_3 model catalyst under high-temperature hydrogen reduction

Xiaoyan Zhong [a], Jing Zhu [a,*], Jingyue Liu [b]

[a] *Electron Microscope Laboratory, School of Materials Science and Engineering, Tsinghua University, Beijing 100084, PR China*
[b] *Monsanto Company, 800 N. Lindbergh Blvd., St. Louis, MO 63167, USA*

Received 18 April 2005; revised 14 June 2005; accepted 18 June 2005

Available online 13 October 2005

Abstract

We investigated the interface structure between the Pt nanoparticles and the alumina support in a Pt/Al_2O_3 model catalyst reduced in flowing hydrogen gas at different temperatures by cross-sectional atomic-resolution transmission electron microscopy nanodiffraction techniques. An interfacial Pt_8Al_{21} alloy with a tetragonal structure was formed at the Pt–alumina interface during the high-temperature reduction at 1073 K. This alloy phase was not formed when the Pt/Al_2O_3 model catalyst was reduced at 773 K. The platinum-assisted reduction of the alumina support and the subsequent strong metal–support interaction at the interface may be responsible for the formation of the interfacial alloy phase.

Keywords: Metal–support interaction; Platinum; Alumina; Interfacial phase; Catalyst; Electron microscopy

1. Introduction

Alumina-supported metal catalysts are widely used in many industrial processes; for example, Ag/α-Al_2O_3 is used to oxidize ethylene to ethylene oxide with high selectivity, Pd/Al_2O_3 provides superior performance as a combustion catalyst, and Pt/Al_2O_3 is widely used as a dual-function catalyst in catalytic reformation of naphtha, as an automotive emission control catalyst, and as a hydrogenation catalyst. One of the main issues in optimizing the performance of these alumina-supported metal catalysts is controlling the size, shape, and spatial distribution of the noble metal particles. To prevent sintering of the noble metal particles during the catalytic reactions at high temperatures and to prolong the lifetime of these commercially important catalysts, we need to understand how the metal particles evolve and interact with the alumina support in various environments at different temperatures.

Understanding the catalytic behaviors of industrial catalysts is a formidable task, because of these catalyst's complex physiochemical nature. It is even difficult—if not impossible—to characterize most of the commercial catalysts. To overcome these difficulties, supported model catalysts, consisting of small metal particles dispersed onto planar single crystal surfaces or thin films, have been introduced [1–7]. These new model catalysts allow the use of surface science techniques to study the effects of the metal, metal–support interaction, support, and even intrinsic cluster size on the performance of supported metal catalysts. For oxide-supported metal catalysts, such as noble metal particles supported on alumina, the key issues are intrinsic cluster-size effects and the metal–support interactions.

In this study we used polycrystalline alumina slabs as the support for our model catalysts. Using polycrystalline oxide materials as substrates has a few advantages over the earlier models that used extremely thin films or single crystals. Metal particles interacting with various surfaces of the oxide support can be treated and studied simultaneously, and the individual oxide grains more closely resemble those used in

* Corresponding author. Fax: +86 10 62772507.
E-mail address: jzhu@mail.tsinghua.edu.cn (J. Zhu).

0021-9517/$ – see front matter
doi:10.1016/j.jcat.2005.06.018

commercial heterogeneous catalysts. We will report detailed studies of polycrystalline oxide materials as substrates for oxide-supported metal catalysts in a future paper.

High-temperature reduction (HTR) of the Pt/Al_2O_3 model catalyst in hydrogen induces enhanced interaction between platinum and alumina. Previous investigations showed that HTR treatment suppressed hydrogenolytic activity [8–14]; it may also affect the selectivity of various catalytic reactions [11,15]. Abasov et al. [16] reported a decreased hydrogen chemisorption capacity of Pt/γ-Al_2O_3 after HTR treatment, as Pt particles became "inaccessible" to hydrogen chemisorption after HTR of hydrogen. In contrast, Den Otter and Dautzenberg [17] attributed the loss of activity to the formation of a Pt–Al alloy. Menon and Froment [12] suggested that the presence of strongly chemisorbed hydrogen caused invalidation of the Pt/Al_2O_3 catalyst after HTR, and Kunimori et al. [18] proposed that the formation of a $Pt \cdot Al_2O_2$ phase at the interfacial region was responsible for the changes in the catalytic properties. It also has been reported that hydrogen can be released from the Pt/Al_2O_3 interface during HTR, leaving platinum in direct contact with the alumina support and thereby shortening the Pt–O bond and thus reducing hydrogen chemisorption capacity [14,19–21]. Using isotopic-labeling temperature-programmed desorption, Aparicio et al. [22] demonstrated that the hydrogen atoms absorbed on the platinum surface migrated to the metal–support interface during HTR treatment. More recent studies by Penner et al. [13,23] demonstrated that the Pt particles, after a reductive treatment at 873 K, interacted with the alumina support to form Pt-rich Pt_3Al particles.

All of these experiments demonstrate the complex nature of $Pt–Al_2O_3$ interactions during HTR of hydrogen and the difficulties in understanding the interfaces (especially the buried interfaces) between the Pt nanoparticles and the alumina support. As part of our study of the interface structures between noble metal particles and the various surfaces of polycrystalline oxides, here we report the direct observation of the interfacial structures and the formation of alloys after HTR treatment of a Pt/Al_2O_3 model catalyst.

To directly study the atomic scale structure of the interfaces between Pt nanoparticles and the alumina support, we developed a protocol for preparing cross-sectional samples of the Pt/Al_2O_3 model catalyst to allow direct observation of the atomic arrangement of the interfaces. We used atomic-resolution transmission electron microscopy (TEM) and electron nanodiffraction techniques to investigate the interface structures and identify the presence of new phases [24,25].

2. Experimental methods

The Pt/Al_2O_3 model catalyst was prepared by electron beam deposition of Pt nanoparticles onto thick ($\sim$ 1 mm) polycrystalline α-Al_2O_3 slabs. The model catalysts were then treated in flowing H_2 (5%)/N_2 gas mixture at the desired temperatures. In this paper we report the experimental results on two model catalysts reduced at 773 and 1073 K for 1 h, then slowly cooled to room temperature. To protect the Pt nanoparticles and their interactions with the alumina support during the sample preparation processes, a thin protective film of amorphous Cr was deposited on each reduced sample.

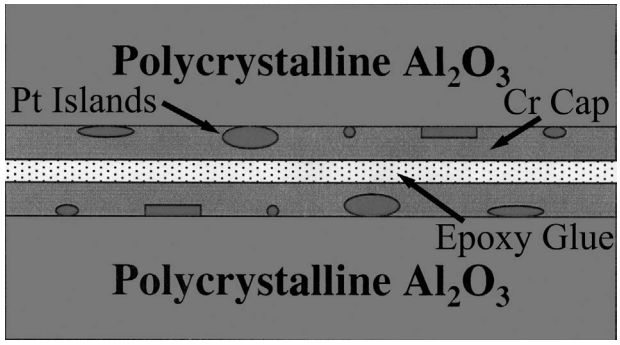

Fig. 1. Schematic cross-sectional TEM sample of a $Pt–Al_2O_3$ model catalyst.

To study the interfacial structures between the Pt nanoparticles and the polycrystalline alumina substrate, we prepared cross-sectional samples by attaching two Pt/alumina slabs with epoxy glue, as shown in Fig. 1. We then sliced the composite sample to expose the cross-sections of the model catalysts, mechanically thinned and polished the slices on both sides to a thickness of about 30 μm, the glued the polished slices to TEM grids for ion milling down to an electron beam-transparent thickness.

We examined both plane-view and cross-sectional samples of Pt/Al_2O_3 model catalysts in a field emission JEM-2010F transmission electron microscope. Atomic-resolution TEM images were digitally recorded with a CCD (charge-coupled device) camera attached to the electron microscope, in which electron diffraction patterns can be obtained from nanometer-scale regions. We used the electron nanodiffraction technique to identify the interfacial interfaces. Both atomic-resolution TEM images and electron nanodiffraction patterns were simulated using standard image simulation software.

3. Results and discussion

3.1. Sintering of Pt nanoparticles

Supported Pt nanoparticles sinter under HTR treatment. The degree of sintering depends on the reduction temperature, gas environment, duration of treatment, and type of substrate. Figs. 2a and c show representative plane-view TEM images of the Pt nanoparticles deposited on the polycrystalline alumina support after reduction in flowing H_2 (5%)/N_2 gas mixture for 1 h at 773 and 1073 K, respectively. The Pt nanoparticles exhibit various shapes. The

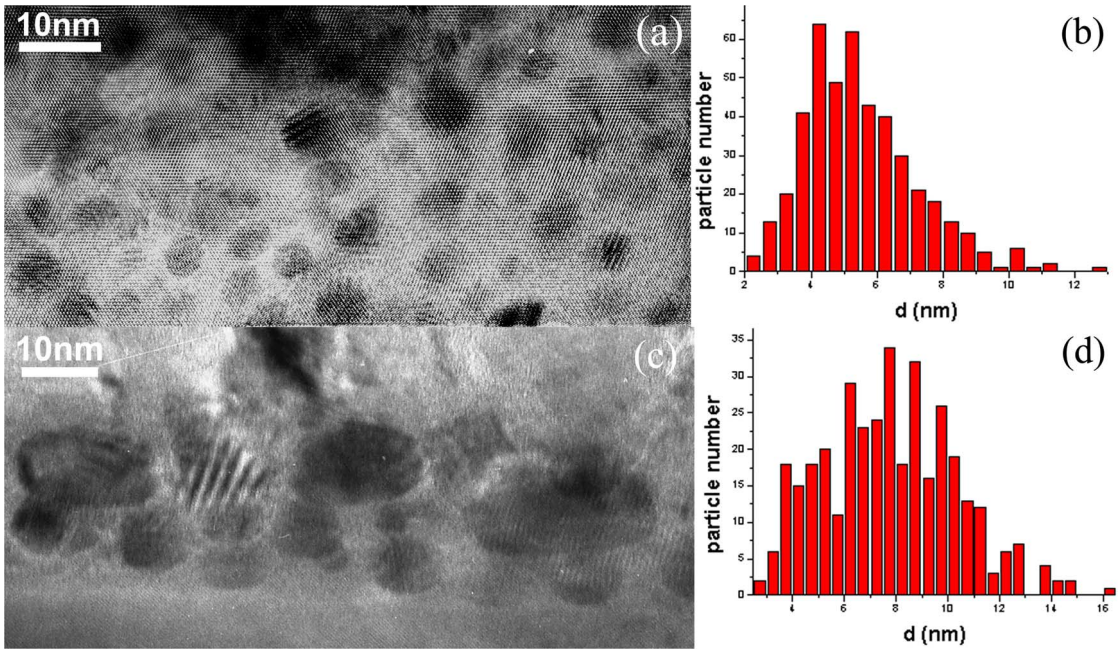

Fig. 2. TEM images of a Pt/Al_2O_3 model catalyst after reduction in H_2/N_2 mixture for 1 h at 773 K (a) and 1073 K (c) showing sintering of Pt nanoparticles at higher reduction temperatures; the corresponding size distributions of the Pt nanoparticles are shown in (b) and (d), respectively.

average particle size is clearly larger at higher reduction temperatures. The shapes of some of the larger particles shown in Fig. 2c suggest that particle–particle coalescence occurred during HTR.

To provide some quantitative measurement on the particle size distributions during the HTR processes, 444 and 361 Pt particles were analyzed from TEM images obtained from the Pt/Al_2O_3 model catalysts reduced at 773 and 1073 K, respectively. Results are given in Figs. 2b and d, respectively. The histograms show that the average diameter of the Pt nanoparticles of the catalyst reduced at 773 K is 5.5 nm, whereas that of the catalyst reduced at 1073 K is 7.7 nm. Furthermore, the size distribution of the Pt nanoparticles is much wider in the 1073 K sample than in the 773 K sample. Increased coalescence occurred at higher-temperature reductions. The degree of Pt sintering also depends on the surface chemistry and the structure of the polycrystalline alumina support. We will report detailed studies on how the degree of sintering of noble metal nanoparticles on the various surfaces of the polycrystalline alumina supports in a separate paper.

3.2. Interfacial structure and formation of interfacial alloy phases

3.2.1. Pt/Al_2O_3 model catalyst reduced at 773 K

Fig. 3 shows a typical cross-sectional high-resolution electron microscopy (HREM) image of the Pt/Al_2O_3 model catalyst reduced at 773 K for 1 h in flowing H_2 (5%)/N_2 gas mixture. The amorphous Cr protective film, Pt particles, and alumina substrate are clearly shown. It seems that Pt nanoparticles are in direct contact with the alumina substrate

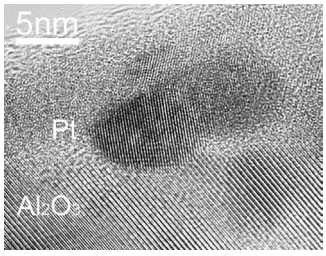

Fig. 3. HRTEM image of a Pt/Al_2O_3 model catalyst after HTR in H_2/N_2 mixture for 1 h at 773 K.

and may preferentially anchor at the steps/kinks/facets of the alumina substrate. Because the substrate is polycrystalline and the Pt particles are deposited on all exposed surfaces of the alumina substrate, no universal epitaxial relationship between the Pt particles and the substrate is observed. Analysis of many HREM images reveals no identifiable interfacial phases at the Pt–alumina interfaces.

3.2.2. Pt/Al_2O_3 model catalyst reduced at 1073 K

Fig. 4 shows a HREM image of the Pt/Al_2O_3 model catalyst after hydrogen reduction at 1073 K, clearly revealing the Cr amorphous film, Pt particles, and alumina substrate with atomic scale resolution. An optical diffractogram of the interfacial regions is shown in the inset at the bottom left of the figure. Detailed examination of the lattice fringes at the interfacial region and the optical diffractogram shows that they are different from those of the α-alumina substrate and the Pt nanoparticle.

The interplanar spacings of the interfacial phase shown in Fig. 4 were 2.15 and 1.39 Å, respectively. The angle between the two crossing planes of the interfacial phase was

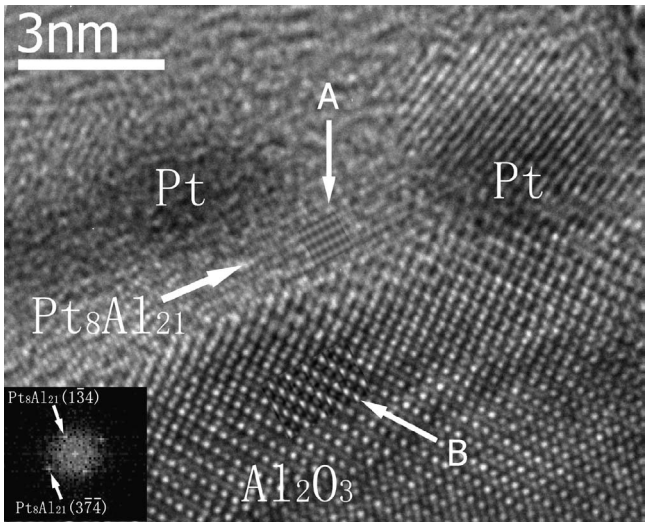

Fig. 4. Atomic resolution TEM image of a cross-section sample of a Pt/Al_2O_3 model catalyst clearly shows the Pt nanoparticles, the structure of the alumina substrate, and the interfacial structures. The sample was reduced in H_2/N_2 mixture for 1 h at 1073 K. The optical diffractogram from the interface region is shown in the inset at the bottom left. Simulated HRTEM images of the interfacial phase Pt_8Al_{21} oriented along the [20 8 1] zone axis and the α-Al_2O_3 substrate oriented along the [010] zone axis were shown in the insets indicated by the letters A and B, respectively.

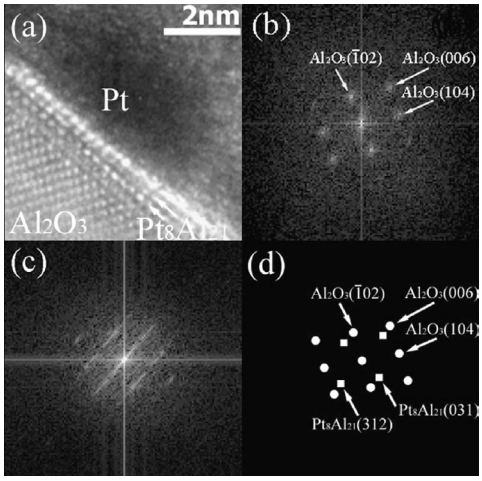

Fig. 5. HRTEM image of the interfacial phase between the Pt nanoparticle and the alumina substrate after HTR at 1073 K for 1 h (a) and the corresponding optical diffractograms obtained from the alumina substrate (b) and from the interface region (c). Schematic diagram (d) depicts the details of the optical diffractogram (c), clearly demonstrating the presence of the Pt_8Al_{21} alloy phase in the interfacial regions.

about 90°. Because Pt–Al alloys can be formed during HTR of Pt/Al_2O_3 catalysts [13,23], we found that the measured spacings and the angle between the cross-planes of the new phase matched the lattice spacings of the (1$\bar{3}$4) and (3$\bar{7}\bar{4}$) planes of the Pt_8Al_{21} alloy with a tetragonal structure. Moreover, the new interface phase was not restricted in the area under the Pt particles, demonstrating that the alumina areas close to Pt particles were also reduced by spillover hydrogen atoms.

Assuming that the new interfacial phase is Pt_8Al_{21} alloy, simulated HREM images, based on the EMS software [26], fit well to the experimental image shown in Fig. 4 if the Pt_8Al_{21} alloy particle is oriented along its [20 8 1] zone axis. The simulated HREM images of the new alloy phase and the α-Al_2O_3 are given in the insets, indicated by "A" and "B," respectively; the simulated images coincide with the experimental images.

Fig. 5a shows another HREM image of the Pt/Al_2O_3 model catalyst in a different region from that shown in Fig. 4. Optical diffractograms obtained from the alumina substrate and the interfacial region (the region enclosed by the dotted line in Fig. 5a), are shown in Figs. 5c and d, respectively. The diffractogram from the interfacial region clearly shows additional diffraction spots. Using lattice fringes of the alumina substrate as an internal calibration, we determined that the additional spots present in the diffractogram obtained from the interracial region represent lattice spacings of 4.12 Å and 3.36 Å with about an 87.5° angle between the planes. The additional set of diffraction spots obtained from the interfacial regions can be indexed as tetragonal Pt_8Al_{21} alloy oriented along the [5$\bar{3}\bar{9}$] zone axis, as shown schematically in Fig. 5d.

Further confirming the presence of the interfacial alloy phase, Fig. 6 shows the electron nanodiffraction patterns obtained from the alumina substrate, the interface, and the Pt particle. The nanodiffraction pattern obtained from the interface clearly shows additional diffraction spots. Using the diffraction patterns from the alumina substrate ([010] zone axis) and the Pt particle as references, we conclude that the additional diffraction spots in Fig. 6b can be indexed as

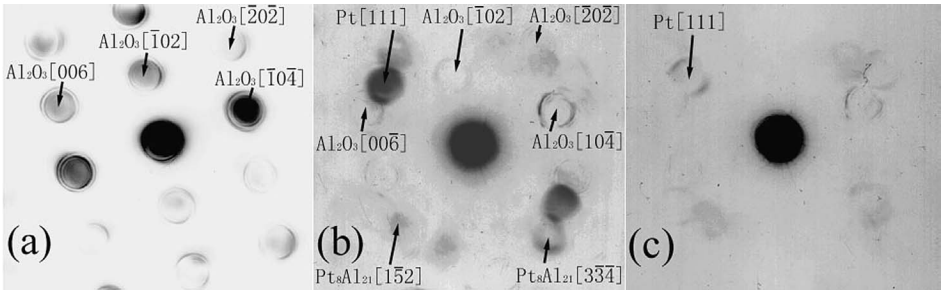

Fig. 6. Nanodiffraction patterns obtained from the substrate (a), an interfacial region (b) and a Pt nanoparticle (c), respectively.

diffraction pattern from a tetragonal Pt_8Al_{21} alloy oriented along the [13 5 6] zone axis.

Analysis of both HREM images and nanodiffraction patterns showed that during the HTR treatment of the Pt/Al_2O_3 model catalyst at 1073 K, a Pt_8Al_{21} alloy phase with a tetragonal structure formed at the interfacial regions between the Pt nanoparticles and the alumina substrate. As discussed earlier, this interfacial alloy phase was not formed during HTR treatment of the Pt/Al_2O_3 model catalyst at 773 K.

Our experiment demonstrates that an interfacial Pt–Al alloy phase is formed at the Pt–Al interfaces when the Pt/Al_2O_3 model catalyst is reduced in hydrogen at 1073 K. Because of hydrogen spillover to the substrate, the interface phase is not limited to the area immediately under the particles. We will be conducting further experiments to investigate the mechanisms of alloy formation and identify any specific relationship between the Pt–Al interfacial interphase with respect to the alumina substrate and Pt nanoparticles. The reduced alumina support during HTR treatment is most probably facilitated by hydrogen spillover from the Pt nanoparticles. At higher reduction temperatures, patches of the alumina support that are in close proximity of the Pt nanoparticles may be reduced to such a degree that the formation of Pt–Al alloy is favored.

4. Conclusion

We identified a tetragonal Pt_8Al_{21} alloy interfacial phase at the Pt–alumina interfaces in the Pt/Al_2O_3 model catalyst after HTR at 1073 K in flowing hydrogen. But we found no alloy phases the Pt/Al_2O_3 model catalyst after HTR at 773 K. The platinum-assisted reduction of the alumina support and the metal–support interaction at the interface have been directly approved by the formation of interfacial-phase Pt_8Al_{21}. We propose that the hydrogen atoms migrating from the Pt particle surface to the metal–support interface induce the reduction of the substrate Al_2O_3, accompanied by the interaction with the metal particles to form the interfacial-phase Pt_8Al_{21}. Because of hydrogen spillover to the substrate, the Pt–Al alloy is formed not only under Pt particles, but also around them. Formation of the Pt–Al alloy phase may have profound effect on the catalytic performance and long-term stability of the Pt/Al_2O_3 model catalyst.

We have demonstrated in this paper that the cross-sectional HREM technique and associated nanodiffraction technique are powerful tools for studying the interface structures of nanoparticles supported on oxide supports. The use of polycrystalline oxide supports will allow us to investigate the relationship of metal particles with respect to the various crystallographic planes of the oxide support under similar synthesis and treatment conditions. Both plane-view and cross-sectional HREM imaging can be used to study the sintering behavior of metal nanoparticles on the various surfaces of oxide supports, as well as the intrinsic nature of the metal–support interfaces. Increased knowledge of the interface structures between metal particles and supports may provide information useful in developing nanostructured heterogeneous catalysts with desired catalytic performance and long-term stability.

Acknowledgments

This work was supported by the National 973 Project of China, the Chinese National Nature Science Foundation, and the National Center for Nanoscience and Technology of China. X.Y. Zhong thanks Professor Furong Chen, National Tsinghua University, for helpful discussions.

References

[1] D.R. Rainer, C. Xu, D.W. Goodman, J. Mol. Catal. A: Chem. 119 (1997) 307.
[2] C.R. Henry, Surf. Sci. Report 31 (1998) 235.
[3] X. Lai, D.W. Goodman, J. Mol. Catal. A: Chem. 162 (2000) 33.
[4] P.L.J. Gunter, J.W.H. Niemantsverdriet, F.H. Ribeiro, G.A. Somorjai, Catal. Rev.-Sci. Eng. 39 (1997) 77.
[5] M. Klimenkov, S. Nepijko, H. Kuhlenbeck, M. Baumer, R. Schlogl, H.-J. Freund, Surf. Sci. 391 (1997) 27.
[6] K. Hayek, M. Fuchs, B. Klotzer, W. Reichl, G. Rupprechter, Top. Catal. 13 (2000) 55.
[7] G. Rupprechter, H.-J. Freund, Top. Catal. 14 (2001) 3.
[8] L. Gonzalez-Tejuka, K. Aika, S. Namba, J. Turkevich, J. Phys. Chem. 81 (1977) 1399.
[9] F.M. Dautzenberg, H.B.M. Wolters, J. Catal. 51 (1978) 26.
[10] M. Vaarkamp, J.T. Miller, F.S. Modica, G.S. Lane, D.C. Koningsberger, in: New Frontiers in Catalysis, Proceedings of 10th International Congress on Catalysis, 19–24 July 1992, Budapest, 1993, p. 809.
[11] R. Karmer, M. Fischbacher, J. Mol. Catal. 51 (1989) 247.
[12] P.G. Menon, G.F. Froment, Appl. Catal. 1 (1981) 31.
[13] K. Hayek, H. Goller, S. Penner, G. Rupprechter, C. Zimmerman, Catal. Lett. 92 (2004) 1.
[14] M. Vaarkamp, J.T. Miller, F.S. Modica, D.C. Koningsberger, J. Catal. 144 (1993) 611.
[15] J. Margitfalvi, P. Szedlacsek, M. Hegedüs, F. Nagy, Appl. Catal. 15 (1985) 69.
[16] S.I. Abasov, V.Y. Borovkov, V.B. Kazansky, Catal. Lett. 15 (1992) 269.
[17] G.J. Den Otter, F.M. Dautzenberg, J. Catal. 53 (1978) 116.
[18] K. Kunimori, Y. Ikeda, M. Soma, T. Uchijima, J. Catal. 79 (1983) 185.
[19] A. Munoz-Páez, D.C. Koningsberger, J. Phys. Chem. 99 (1995) 4193.
[20] D.C. Koningsberger, M. Vaarkamp, Physica B 208–209 (1995) 633.
[21] M. Vaarkamp, J.T. Miller, F.S. Modica, D.C. Koningsberger, J. Catal. 163 (1996) 294.
[22] P.F. Aparico, A.G. Ruiz, I.R. Ramos, J. Chem. Soc., Faraday Trans. 93 (1997) 3563.
[23] S. Penner, D. Wang, D.S. Su, G. Rupprechter, R. Podloucky, R. Schlögl, K. Hayek, Surf. Sci. 276 (2003) 532.
[24] J. Zhu, J.M. Cowley, Acta Crystallogr. 38 (1982) 718.
[25] D. Wang, S. Penner, D.S. Su, G. Rupprenchter, K. Hayek, R. Schlögl, J. Catal. 219 (2003) 434.
[26] P. Stadelmann, Ultramicroscopy 21 (1987) 131.